Modelling of the Wall Effect in Packed Bed Adsorption

By Witold Kwapinski, Markus Winterberg, Evangelos Tsotsas, and Dieter Mewes*

A model developed for catalytic packed bed reactors and consistently accounting for the influence of the tube wall on porosity, flow and transport phenomena is used in order to simulate the operation of packed bed adsorbers. By comparison of simulation results with reduced versions of the model the influence of the wall on adsorber performance is worked out and found to be major at low ratios between tube and particle diameter. The interaction between maldistribution, thermal effects and intraparticle resistances in such adsorber tubes is discussed.

1 Introduction

Separation, cleaning and drying of gas mixtures by adsorption in packed beds find broad application in the process, chemical and environmental industry. Due to intensive research, the physical fundamentals of adsorption are relatively well understood, and the prediction of breakthrough in packed beds with a large tube-to-particle diameter ratio, D/d_p, is possible with sufficient accuracy (see, e.g., [1,2]).

The situation is more difficult with relatively slim tubes, since at small D/d_p ratio the tube wall has a considerable influence on porosity, fluid flow, heat transfer and mass transfer in the bed. This wall influence was investigated for isothermal [3-8], in some cases also for non-isothermal adsorption [9,10]. However, the respective models often include simplifying assumptions (specific types of adsorption equilibrium, constant pattern behavior, lumped overall coefficients for fluid-to-particle mass transfer). Many authors use porosity profiles $\psi(r)$ with an only weak rise of porosity to the wall. In the computation of the flow profile $u_0(r)$ nearly all authors work with the fluid viscosity instead of an increased effective viscosity. Giese et al. [11,12] have shown that the conditions of flow through the bed are not realistically described in this way. Still more unrealistic or at least more uncertain are calculations of the radial dispersion coefficient $D_r(r)$ and the radial effective thermal conductivity $\Lambda_r(r)$. These functions are calculated on the basis of correlations derived with plug flow models, by typically replacing the average by the local flow velocity. Only Lingg [9] tries to express the radial effective thermal conductivity as a function of the radial coordinate, using, however, relationships that are, from the present point of view, not up-to-date.

Therefore, the main objective of the present work is to revisit by simulations the influence of tube wall on packed bed adsorption. To this purpose, recently developed models are used, which are proven by extensive validation to very reliably describe heat and mass transfer, and the operation of wall-cooled catalytic packed bed reactors [13-18]. Such models are based on a consistent description of the radial profiles of porosity, flow, dispersion and conductivity in the bed. First, the models are presented, cast in a form that allows for the treatment of packed bed adsorption. Reduced model versions are also derived, for the sake of comparison and reference. Second, the numerical solution and its validation are discussed. Finally, selected simulation results for isothermal and non-isothermal adsorption are presented and analyzed.

The investigated parametric space is oriented to the adsorption of water vapor from air on 4A zeolite. Separate measurements on single particles have provided adsorption kinetics and equilibria for this material system [19]. Respective data are taken over from [19], along with a simple model for fluid-to-particle mass transfer, and will not be repeated here. On the other hand, packed bed dimensions are oriented to experimental investigations, which are presently in progress and

[*] Dr.-Ing. W. Kwapinski (witold.kwapinski@vst.uni-magdeburg.de), Prof. Dr.-Ing. habil. E. Tsotsas, Thermal Process Engineering, Otto-von-Guericke-University Magdeburg, Universitaetsplatz 2, 39106 Magdeburg, Germany; Dr.-Ing. M. Winterberg, Degussa AG – Engineering, Paul-Baumann-Str. 1, 45764 Marl, Germany, Prof. Dr.-Ing. habil. Dieter Mewes, Process Engineering, University Hannover, Callinstr. 36, 30617 Hannover, Germany

implement near infra-red tomography for the temporal and spatial resolution of breakthrough at the outlet of the bed [20]. Respective comparisons will be published at due time.

2 Maldistribution of Porosity and Flow

Based on the work by Giese [11], the radial porosity profile in the packed tube is calculated by the monotonic exponential expression

$$\psi(r) = \psi_\infty \left[1 + 1.36 \exp\left(-5.0 \frac{R - r}{d_p} \right) \right] \tag{1}$$

with R = D/2. Equation (1) is valid for particles that are nearly – but not perfectly – monodispersed and nearly – but not perfectly – spherical in shape. Its integration over the radial coordinate, r, leads to the average porosity, $\overline{\psi}$, of beds confined in cylindrical tubes. In the present work, the average porosity of a bed with D/d_p = 11 has been measured to $\overline{\psi}$ = 0.405, and the porosity at infinite distance from the wall has been derived to ψ_∞ = 0.365. It should be stressed that $\overline{\psi}$ changes with D/d_p, while ψ_∞ does not.

Higher porosity in the vicinity of the walls leads to higher velocities in this region of the tube that extends over about half a particle diameter from the wall. The lower the tube-to-particle diameter ratio, the more pronounced the deviation from uniform flow (plug flow). The increase of flow velocity in the vicinity of the wall is accompanied, due to continuity, by a decrease in the middle of the bed. The velocity profile is calculated by means of the extended Brinkman equation

$$\frac{\partial p}{\partial z} = -f_1 u_0(r) - f_2 [u_0(r)]^2 + \frac{\eta_{eff}}{r} \frac{\partial}{\partial r} \left(r \frac{\partial u_0}{\partial r} \right), \tag{2}$$

with

$$f_1 = 150 \frac{[1 - \psi(r)]^2}{[\psi(r)]^3} \frac{\eta_f}{{d_p}^2}, \tag{3}$$

$$f_2 = 1.75 \frac{[1 - \psi(r)]}{[\psi(r)]^3} \frac{\rho_f}{d_p}, \tag{4}$$

the effective viscosity after Giese

$$\frac{\eta_{eff}}{\eta_f} = 2.0 \exp\left(3.5 \cdot 10^{-3} \, Re_0 \right), \tag{5}$$

the Reynolds number

$$Re_0 = \frac{\overline{u}_0 \, d_p}{\nu_f}, \tag{6}$$

and the boundary conditions

$z = 0$ then $p = p_{in}$,

r = 0 then $\frac{\partial u_0}{\partial r} = 0$,
r = R then $u_0 = 0$.

The first two terms on the right-hand side of eq.(2) account for head loss caused by the particles and are widely known as D'Arcy and quadratic or Ergun term, respectively. The third term describes the head loss resulting from viscous friction in the vicinity of the wall and combines with the no slip boundary condition ($u_0 = 0$). Since porosity and velocity profiles obtained from the above equations have often been presented in literature [11-18], we refrain here from respective plots.

3 Packed Bed Models

The transcription of the packed bed model after [13], see also [14-18], for adsorption is, concerning mass transfer

$$\psi(r)\frac{\partial Y}{\partial t} = \frac{1}{r}\frac{\partial}{\partial r}\left[D_r(r) r \frac{\partial Y}{\partial r} \right] + D_{ax}(r)\frac{\partial^2 Y}{\partial z^2} - u_0(r)\frac{\partial Y}{\partial z} - \left[1-\psi(r)\right]\frac{\partial X}{\partial t}\frac{\rho_p}{\rho_f} \quad . \tag{7}$$

The change of mass of adsorbate with time is accounted for in the last term on the right-hand side of eq.(7) according to the model from [19]. In this two-layers model, gas-side and particle-side mass transfer are described by separate coefficients, β_f resp. β_p, without calculating the intraparticle concentration field. The previously discussed radial profiles of porosity and flow velocity are implemented in eq.(7). Axial dispersion coefficients are calculated locally as

$$D_{ax}(r) = \delta_{bed}(r) + \frac{Pe_0}{2}\delta \tag{8}$$

with

$$Pe_0 = \frac{\bar{u}_0\, d_p}{\delta} \quad . \tag{9}$$

The variation of the radial dispersion coefficient with the radial coordinate is expressed by the relationship

$$D_r(r) \;=\; \delta_{bed}(r) + K_1\, Pe_0\, \frac{u_c}{\bar{u}_0}\, f(R-r)\,\delta \tag{10}$$

with the function

$$f(R-r) \;=\; \begin{cases} \left(\dfrac{R-r}{K_2\, d_p}\right)^2 & \text{for} \quad 0 \le R-r \le K_2\, d_p \\ 1 & \text{for} \quad K_2\, d_p < R-r \le R \end{cases} \quad , \tag{11}$$

which includes the slope parameter

$$K_1 = \frac{1}{8}\left(1 + \frac{3}{\sqrt{Pe_0 u_c / u_0}}\right)^{-1} \tag{12}$$

and the damping parameter

$$K_2 = 0.44 \; . \tag{13}$$

The slope parameter describes how dispersion increases with increasing intensity of cross-mixing at higher molecular Péclet numbers, Pe_0. The function f(R-r) and the damping parameter describe the inhibition of cross-mixing in the vicinity of the wall.

The analogous equation for heat transfer is

$$\begin{aligned}\left\{\psi\rho_f c_f + \left[1-\psi\right]\rho_p c_p\right\}\frac{\partial T}{\partial t} &= \frac{1}{r}\frac{\partial}{\partial r}\left[\Lambda_r(r) r \frac{\partial T}{\partial r}\right] + \Lambda_{ax}(r)\frac{\partial^2 T}{\partial z^2} - u_0(r)\rho_f c_f \frac{\partial T}{\partial z} \\ &- \left[1-\psi(r)\right]\Delta H_{ad}\rho_p \frac{\partial X}{\partial t} \; ,\end{aligned} \tag{14}$$

with the effective axial thermal conductivity

$$\Lambda_{ax}(r) = \lambda_{bed}(r) + \frac{Pe_0}{2}\lambda_f \; , \tag{15}$$

the molecular Péclet number for heat transfer

$$Pe_0 \;\; = \;\; \frac{\bar{u}_0 \, \rho_f \, c_f \, d_p}{\lambda_f} \; , \tag{16}$$

and the effective radial thermal conductivity

$$\Lambda_r(r) \; = \lambda_{bed}(r) + K_1 \, Pe_0 \, \frac{u_c}{\bar{u}_0} \, f(R-r) \, \lambda_f \; . \tag{17}$$

The damping function f(R-r) remains the same as for mass transfer (eq.(11)), while the slope parameter and the damping parameter are slightly modified to, respectively,

$$K_1 = \frac{1}{8} \; , \tag{18}$$

$$K_2 = 0.44 + 4\exp\left(-\frac{Re_0}{70}\right) . \tag{19}$$

The heat release by adsorption, see [19] for ΔH_{ad}, is derived in the last term on the right-hand side of eq.(14) from the change of solids load with time. This very term couples the energy with the mass balance, so that both have to be solved simultaneously in order to account for thermal effects. Heat transfer resistances to or in the particles are neglected. The terms $\delta_{bed}(r)$ and $\lambda_{bed}(r)$ in eqs (8), (10), (15) and (17) describe the isotropic effective diffusivity and thermal conductivity of the bed without fluid flow. Boundary and initial conditions for eqs (7) and (14) are recapitulated in Table 1.

On the basis of the above general model various reductions are possible by neglecting thermal effects, the radial coordinate or gas-to-particle and intraparticle mass transfer resistances. From such reduced versions the following have been considered in more detail in the present work:

1) plug-flow model (1-D) with local equilibrium between the gas and the solids,
2) plug-flow model (1-D) with mass transfer resistance to the solids,
3) 2-D maldistribution model with local equilibrium,
4) 2-D maldistribution model with mass transfer resistance to the solids.

In our terminology "plug flow" means that every influence of the radial coordinate is neglected, including the influence of the wall on porosity and flow velocity. However, axial dispersion, as expressed by the dispersion coefficient D_{ax}, is accounted for, so that the equation

$$\overline{\psi}\frac{\partial Y}{\partial t} = D_{ax}\frac{\partial^2 Y}{\partial z^2} - \overline{u}_0\frac{\partial Y}{\partial z} - \left[1-\overline{\psi}\right]\frac{\partial X}{\partial t}\frac{\rho_p}{\rho_f} \tag{20}$$

applies to the isothermal plug flow models (models 1 and 2). Equation (20) is the classical, conventional way to model packed bed adsorbers. Local equilibrium corresponds, in terms of the two-layers model from [19], to the limiting case of $\beta_f \to \infty$ and $\beta_p \to \infty$. At this limit, equilibrium is considered to be sufficient for calculating the response of the solid phase to changes of the concentration in the fluid. Model 4 is our complete, highest order model, as previously outlined and in exact correspondence to [13-18]. Mainly this model has been evaluated for both isothermal and non-isothermal conditions.

4 Numerical Solution and its Validation

The partial differential equation or equations of the various models have been solved by the method of lines. The numerical calculations were conducted for different mesh densities, and the results accepted when the change of calculated gas moisture content values was lower than 0.05 % of the maximal difference of gas moisture content appearing in the packed bed. When the error was bigger, the mesh was made denser. Since the width of the concentration front is, in many cases, not much smaller than the length of the bed, equidistant meshes have been used in the axial direction. In the maldistribution models (models 3 and 4 in previous section) meshes that were denser near the wall than in the center of the tube have been applied.

To check the numerical procedure, respective results have been compared with available analytical solutions. One such solution is attributed to Anzelius [1] and refers to model 2 after the classification of section 3, additionally reduced by neglecting axial dispersion ($D_{ax} = 0$). Furthermore, it is assumed that the sorption equilibrium is throughout linear ("Henry's law"), and that the bed is long. The mass transfer resistance is attributed to the fluid phase. Then, axial profiles can be derived to

$$\frac{C}{C_{in}} = \frac{1}{2}\operatorname{erfc}\left(\sqrt{\xi} - \sqrt{\tau}\right), \tag{21}$$

with

$$\xi = 6\frac{\beta_f}{d_p}\frac{z}{u}\frac{1-\psi}{\psi}, \tag{22}$$

and

$$\tau = 6\frac{\beta_f}{d_p K}\left(t - \frac{z}{u}\right). \tag{23}$$

In eq.(21) the concentration of adsorbate in the gas phase, C, is used instead of the content, Y, assuming an initial value of $C_0 = 0$. In eqs (22), (23) the equilibrium constant (slope of the isotherm) is denoted by K, while u is the interstitial flow velocity ($u = u_0/\psi$). Bars are not used to denote averages (compare with eq.(20)), for the sake of simplicity.

The numerical results are in very good agreement with analytical solutions for different mass transfer coefficients, as Fig. 1 shows. Only for the smallest value of the mass transfer coefficient, β_f, a certain deviation is conceivable. The reason lies not in the numerical, but in the analytical solution, which is valid only for long beds – long in dimensionless terms, as expressed by the value of the parameter ξ. The fact that ξ becomes too small with decreasing β_f can be remediated by increasing z. Excellent agreement can be obtained at any mass transfer coefficient, provided that the adsorber is long enough.

If the mass transfer to the particles is neglected and, instead, axial dispersion considered, model 1 from section 3 is obtained. Assuming, again, linear equilibrium and long times of retention the so-called Levenspiel and Bischoff solution is derived (see [1]) to

$$\frac{C}{C_{in}} = \frac{1}{2}\,\mathrm{erfc}\left[\frac{1-\frac{\bar{t}}{\bar{t}}}{2\left(\frac{D_{ax}}{u\psi z}\frac{\bar{t}}{\bar{t}}\right)^{0.5}}\right], \tag{24}$$

where

$$\bar{t} = \frac{z}{u}\left(1 + K\frac{1-\psi}{\psi}\right). \tag{25}$$

While eqs (24) and (25) are explicit in terms of breakthrough, they can also be used to calculate axial concentration profiles, as depicted in Fig. 2. Small deviations in the comparison with numerical results can, once more, be removed by giving to the front the opportunity to move further downstream [21]. Asymptotically, the so-called primary transfer function is obtained, and the influence of boundary conditions vanishes completely. This influence is still conceivable in Fig. 2, where numerical results for both $C = C_{in}$ (or $Y = Y_{in}$, "zero BC") and the more complicated boundary condition after Danckwerts at $z = 0$ (see Table 1) are given. Since the influence is small, the simpler, zero boundary condition will be used in calculations with the maldistribution models.

5 Wall effect in isothermal adsorption

From many conducted simulations only a few selected results will be presented and discussed here. All respective calculations were made for adsorption of water vapour on 4A zeolite particles [19] packed in a cylindrical tube with D = 50 mm. Gas properties are determined at 25 °C.

Figure 3 shows exemplarily calculated axial profiles of average gas moisture content along the adsorber for all isothermal models stated in section 3 and recapitulated in the legend of the figure. It should be stressed that $\overline{Y}$ takes locally different flow velocities into consideration, that means it is a mixing cup average, turned dimensionless by the initial and inlet gas moisture contents, Y_0 and Y_{in}, respectively. The curves have been gathered together in Fig. 3 by defining the abscissa as $z\text{-}z_R$, wherein z_R is the individual midpoint of every curve, corresponding to an ordinate value of 0.5. Comparison of the plug flow with the maldistribution models (i.e. comparison of model 1 with 3, or model 2 with 4) shows that by consideration of the wall effect the curves become flatter and spread out. Consequently, what we macroscopically interpret as "axial dispersion" is – to a certain part – not due to D_{ax}, mass transfer resistances or to equilibrium, but caused by the radial distributions of porosity, flow velocity and effective transport coefficients in the packed bed. The lower the ratio D/d_p, the larger is this contribution to the second moment of the profiles, as Fig. 4 points out.

Obviously, the usual assumption of uniform flow (plug flow) would cause major mistakes at diameter ratios smaller than about 20. This value copes well with existing experience from packed bed reactors. However, in both cases of adsorption and catalysis it depends on a multitude of further operating parameters and material properties, so that a clear limit for the applicability of plug flow approaches can not be declared.

The same data as in Fig. 3 are plotted in Fig. 5a, though this time versus the actual axial coordinate, z. The comparison reveals that, independently of whether mass transfer resistances are considered or not, the plug flow models lead to profiles with the same midpoint, i.e. they have the same average retention time. This is not true for their comparison with the maldistribution models. Consequently, not only the second moment, but also the first moment of the curves is influenced, to a certain extent, by the disturbance of the bed caused by the rigid wall.

Figure 5a (as all the others except Fig. 5b) has been calculated with the isotherms for adsorption of water vapor on zeolite after [19] in their still convex part. Such Langmuir-like ("type II") equilibria are called favorable, because they inhibit the increase of the second moment of concentration profiles or breakthrough curves and, in this sense, compete with the already mentioned dispersive mechanisms. The wall effect must be counted to such dispersive mechanisms, as already discussed. Indeed, constant pattern behavior arises in case of Fig. 5a for all models. Consequently, the profiles do not change any more after a certain inlet transient, but move translatorially through the bed. Without dispersive mechanisms, favorable equilibrium would transform any inlet signal between two distinct concentration levels to a shock wave. Such simulations have also been conducted and are, numerically, extremely demanding, because solution errors increase with increasing steepness of the concentration front. In the calculations of Fig. 5b a throughout linear equilibrium has been assumed, so that the observable dispersion is much larger than in Fig. 5a. Constant pattern behavior is not obtained in this case.

Local gas moisture content profiles calculated after the isothermal version of the maldistribution model with mass transfer resistance (model 4 from section 3) at the center of the tube as well as at a position near the wall are shown in Fig. 6. We see that the gas moisture content profiles in the vicinity of the wall have moved further than those in the bed center, due to near-wall flow channeling. The lag between center and near-wall profiles increases with decreasing diameter ratio, D/d_p. For many practical applications one would have to design rather on the basis of wall gas moisture content profiles and breakthrough curves in order to be on the safe side, with a considerably lower adsorption capacity and operation time before switching to desorption. Reduction of D/d_p increases the second moment of the gas moisture content profiles at both the center and the margin of the tube.

In spite of their importance, maldistribution effects are in case of packed bed adsorption only one component of a complex behavior. Another important component is, as already indicated by Fig. 3, the mass transfer resistance between the mobile and the stationary phase. For the investigated material system this mass transfer resistance is located primarily in the particles [19]. The lower the particle mass transfer coefficient, β_p, the flatter and more spread out is the concentration curve.

6 Combined wall and thermal effects in non-isothermal adsorption

In many cases, especially at highly loaded feeds, the adsorption process in the fixed bed is strongly exothermic. Not only concentration but also temperature profiles will then migrate through the porous medium, and have to be modeled by consideration of the energy balance, as described in section 3. Selected non-isothermal calculations conducted with the parameters of Table 2 will be presented in the following. As Table 2 shows, the wall temperature has been assumed to be equal to the gas inlet temperature in these calculations. The temperature dependence of adsorption equilibrium and of intraparticle mass transfer [19] is accounted for.

Figure 7 shows breakthrough curves in the core and at the wall of the adsorber calculated at different D/d_p ratios by means of the non-isothermal model with mass transfer resistance.

Calculations were also made for the isothermal mode (Fig. 8), with otherwise the same parameters. The comparison reveals completely different positions and slopes of the breakthrough curves. In case of isothermal operation, near-wall breakthrough is faster than the breakthrough in the center of the adsorber at any value of D/d_p. In the non-isothermal case, the same is true only for the lower value of D/d_p. At higher values of the diameter ratio there can be a part of the adsorber where the concentration is higher in the core than in the near-wall region.

The same effect is clearly visible in Fig. 9, where the complete concentration field in the adsorber is depicted at a specified time. The flow maldistribution in the vicinity of the wall causes higher concentration and loading in this region than in the core for the ratio $D/d_p = 11$. However, for a higher ratio of $D/d_p = 25$ the moisture content of the gas can be larger in the core region than near the wall. In this case, the effect of maldistribution does not dominate, but is overlapped by the reduction of adsorption capacity due to the increase of temperature in the core of the bed. Obviously, maldistribution and the non-isothermal character of the process interact in a complex way. Characteristic of the thermal influence is also the fact that adsorption is completed after 10000 s according to Fig. 8, while it is still going on according to Fig. 7.

The temperature field in the adsorber is exemplified in Fig. 10 for the diameter ratio $D/d_p = 11$. The temperature decreases in the radial direction because of cooling of the wall at the temperature of inlet gases. In axial direction, temperature grows at the entrance region of the adsorber till a maximum is reached (a hot spot, as with exothermic catalytic reactions), and falls then because of decreasing concentration of moisture in the gas and wall cooling. The temperature profiles depend only moderately on D/d_p, provided that this ratio is varied by changing the particle, and not the tube diameter. They become flatter and spread out with increasing time.

7 Conclusions

A two-dimensional model for heat and mass transfer in packed beds has been used to simulate adsorption under severe operating conditions of high load, and high wall and thermal effects. The model does not only consider the increase of porosity and flow velocity near the tube wall, but also expresses the effective transport coefficients as functions of the radial coordinate. It has been extensively validated for the case of pure transport phenomena, or wall-cooled, catalytic packed bed reactors, and helps to avoid oversimplifying assumptions and inconsistencies of previous modelling approaches.

The investigated parametric space is oriented to the adsorption of water vapour from air on 4A zeolite. Separate measurements of adsorption kinetics and equilibria on single particles are available for this material system and have been used. The accuracy of numerical calculation has been documented by comparison with existing analytical solutions. Reduced models have been solved for the purpose of comparison. The simulation results and their analysis reveal that the described two-dimensional modelling is mandatory in order to reliably represent the operation of packed bed adsorbers with tube-to-particle diameter ratios of less than about twenty. Such adsorbers can not be treated with conventional, one-dimensional approaches. Wall (channelling) effects, thermal effects and the influence of intraparticle kinetics combine in the investigated region of operating conditions in an intimate and complex way. At present, a novel near infra-red tomographic technique is applied in order to measure breakthrough curves with the spatial and time resolution necessary for detailed comparison with the results of the simulations.

Acknowledgment

The authors gratefully acknowledge financial support by the Deutsche Forschungsgemeinschaft (DFG).

Symbols used

c	[J/(kg·K)]	heat capacity
C	[mol/m^3]	concentration
d	[m]	diameter
D	[m]	diameter of the adsorber
D	[m^2/s]	effective mass dispersion coefficient
L	[m]	bed length
ΔH	[J/kg]	isosteric heat
K	[-]	slope of isotherm
p	[Pa]	pressure
r	[m]	radial coordinate
R	[m]	radius
t	[s]	time
T	[K], [°C]	temperature
u	[m/s]	interstitial velocity
u_0	[m/s]	superficial velocity
u_c	[m/s]	superficial core velocity
X	[kg/kg $_{dry}$]	solids moisture content
Y	[kg/kg $_{dry}$]	gas moisture content
z	[m]	axial coordinate

Greek Symbols

β	[m/s]	mass transfer coefficient
δ	[m^2/s]	diffusion coefficient
η	[Pa·s]	dynamic viscosity
λ	[W/(m·K)]	thermal conductivity
Λ	[W/(m·K)]	effective thermal conductivity
ν	[m^2/s]	kinematic viscosity
ρ	[kg/m³]	density
φ	[-]	relative humidity
ψ	[-]	porosity

Subscripts

ad	adsorption, adsorbate
ax	axial
bed	bed
c	core
eff	effective
f	fluid
in	gas inlet
p	particle
r	radial
R	retention, midpoint of front
w	wall
0	initial, reference, superficial
–	average

∞ at infinite distance from the wall

References

[1] D.M. Ruthven, *Principles of Adsorption and Adsorption Processes,* Wiley-Interscience, New York **1984**.
[2] W. Kast, *Adsorption aus der Gasphase,* VCH, Weinheim **1988**.
[3] Vortmeyer, D., Michael, K., *Chem. Eng. Sci.* **1985**, 40, 2135.
[4] J. Tobis, D. Vortmeyer, *Chem. Eng. Sci.* **1988**, 43, 1363.
[5] J. Tobis, D. Vortmeyer, *Chem. Eng. Process.* **1991**, 29, 147.
[6] R. Germerdonk, A. Wang, *Chem. Eng. Process.* **1993**, 32, 359.
[7] D. Vortmeyer, M.Giese, G. Lingg, *Chem. Eng. Sci.* **1994**, 49, 2593.
[8] O. Bey, *Strömungsverteilung und Wärmetransport in Schüttungen*, Dissertation, Universität Stuttgart, Nr. 570, VDI Fortschr. Ber., Düsseldorf **1998**.
[9] G. Lingg, *Die Modellierung gasdurchströmter Festbettadsorber unter Beachtung der ungleichmäßigen Strömungsverteilung und äquivalenter Einphasenmodelle*, Dissertation, TU München **1995**.
[10] H.J. Bart, R. Germerdonk, P. Ning, *Chem. Eng. Process.* **1996**, 35, 57.
[11] M. Giese, *Strömung in porösen Medien unter Berücksichtigung effektiver Viskositäten*, Dissertation, TU München **1998**.
[12] M. Giese, K. Rottschäfer, D. Vortmeyer, *AIChE J.* **1998**, 44, 484.
[13] M. Winterberg, E. Tsotsas, A. Krischke, D. Vortmeyer, *Chem. Eng. Sci.* **2000**, 55, 967.
[14] M. Winterberg, E. Tsotsas, *Chem. Eng. Sci.* **2000**, 55, 5937.
[15] M. Winterberg, E. Tsotsas, *Int. J. Therm. Sci.* **2000**, 39, 556.
[16] M. Winterberg, E. Tsotsas, *AIChE J.* **2000**, 46, 5.
[17] E. Tsotsas, Section Dee in *VDI-Waermeatlas*, 9th ed., Springer, Berlin **2002**.
[18] E. Tsotsas, chapter 2.8 in *Heat Exchanger Design Update*, Begell House Inc., New York **2000**.
[19] W. Kwapinski, E. Tsotsas, *Chem. Eng. Technol.* **2004**, 27, 681.
[20] K. Salem, D. Mewes, E. Tsotsas, *Proceedings of 3rd World Congress on Industrial Process Tomography*, Banff, Canada, **2003**, 199.
[21] A. Seidel-Morgensrern, *Chem. Eng. Sci.* **1991**, 46, 2567.

Received…

Table 1. Boundary and initial conditions for models.

$t > 0$	$0 \leq r \leq R$	$z = 0$		$Y=Y_{in}$ or $u_0(Y_{in} - Y) = -D_{ax}\frac{\partial Y}{\partial z}$	$T=T_{in}$
		$z=L$	$\frac{\partial X}{\partial z} = 0$	$\frac{\partial Y}{\partial z} = 0$	$\frac{\partial T}{\partial z} = 0$
$t > 0$	$0 \leq z \leq L$	$r=0$	$\frac{\partial X}{\partial r} = 0$	$\frac{\partial Y}{\partial r} = 0$	$\frac{\partial T}{\partial r} = 0$
		$r=R$	$\frac{\partial X}{\partial r} = 0$	$\frac{\partial Y}{\partial r} = 0$	$T=T_w$
$t = 0$	$0 \leq r \leq R$	$0 \leq z \leq L$	$X(r,z) = X_0$	$Y(r,z) = Y_0$	$T(r,z) = T_0$

Table 2. Conditions for calculations with the non-isothermal model; (not mentioned parameters were the same as in the previous, isothermal calculations).

$\bar{u}_0$	[m/s]	0.034
φ_0	[-]	0.252
φ_{in}	[-]	0.523
T_{in}	[K]	314
T_w	[K]	314
λ_p	[W/(m·K)]	0.1

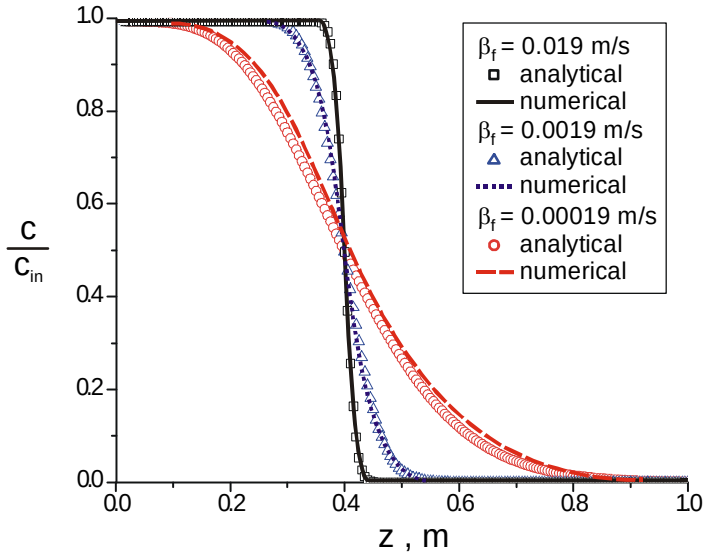

Figure 1. Comparison of numerical results with asymptotic analytical solutions accounting for gas-particle mass transfer. Calculations were made for the following conditions: $u_0 = 0.1$ m/s, $\psi = 0.4$ and $K = 4700$.

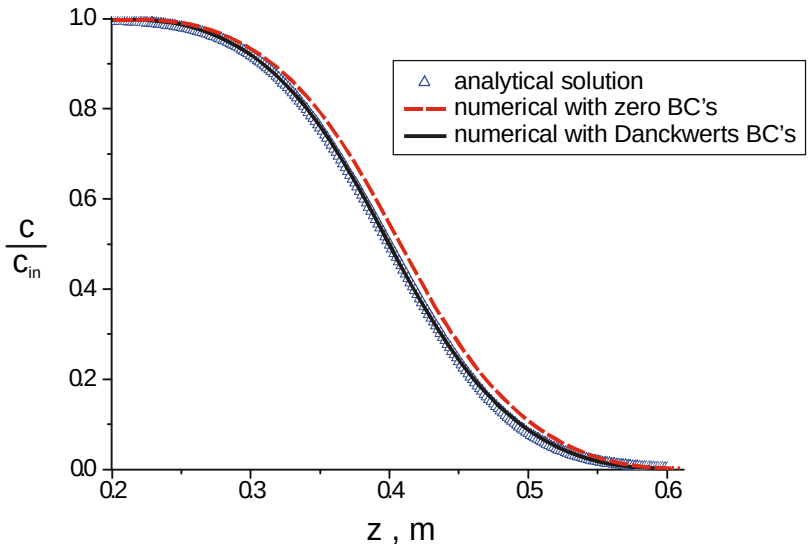

Figure 2. Comparison of asymptotic analytical solutions accounting for axial dispersion with numerical results with different boundary conditions. Calculations were made for the same parameters as in Fig. 1.

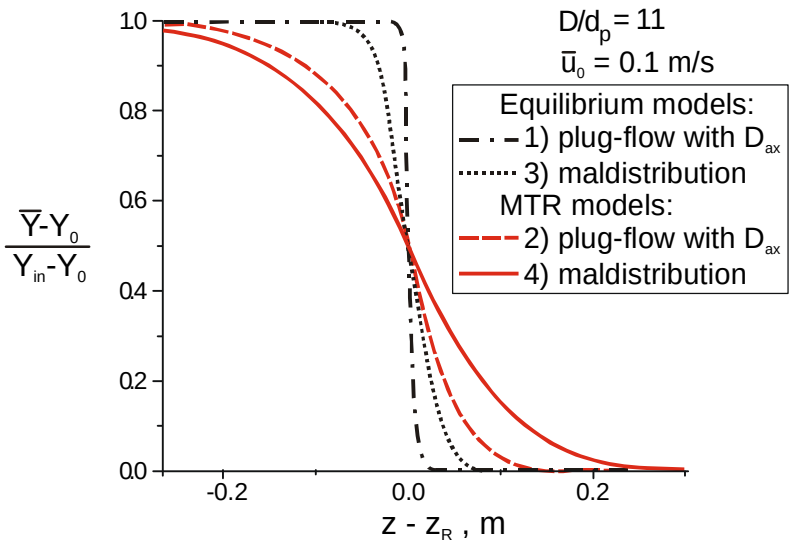

Figure 3. Comparison of axial profiles of average gas moisture content for (1) plug flow model with local equilibrium, (2) plug-flow model with mass transfer resistance, (3) maldistribution model with local equilibrium, and (4) maldistribution model with mass transfer resistance; ($\varphi_0 = 0.05$, $\varphi_{in} = 0.60$, $t = 3 \cdot 10^4$ s).

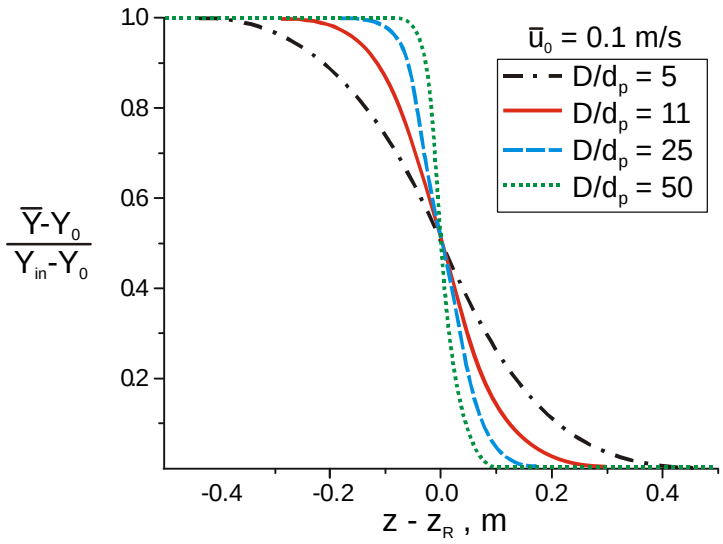

Figure 4. Comparison of axial profiles of average gas moisture content for the maldistribution model with mass transfer resistance at different tube-to-particle diameter ratios. Calculations were made for otherwise the same conditions as in Fig. 3.

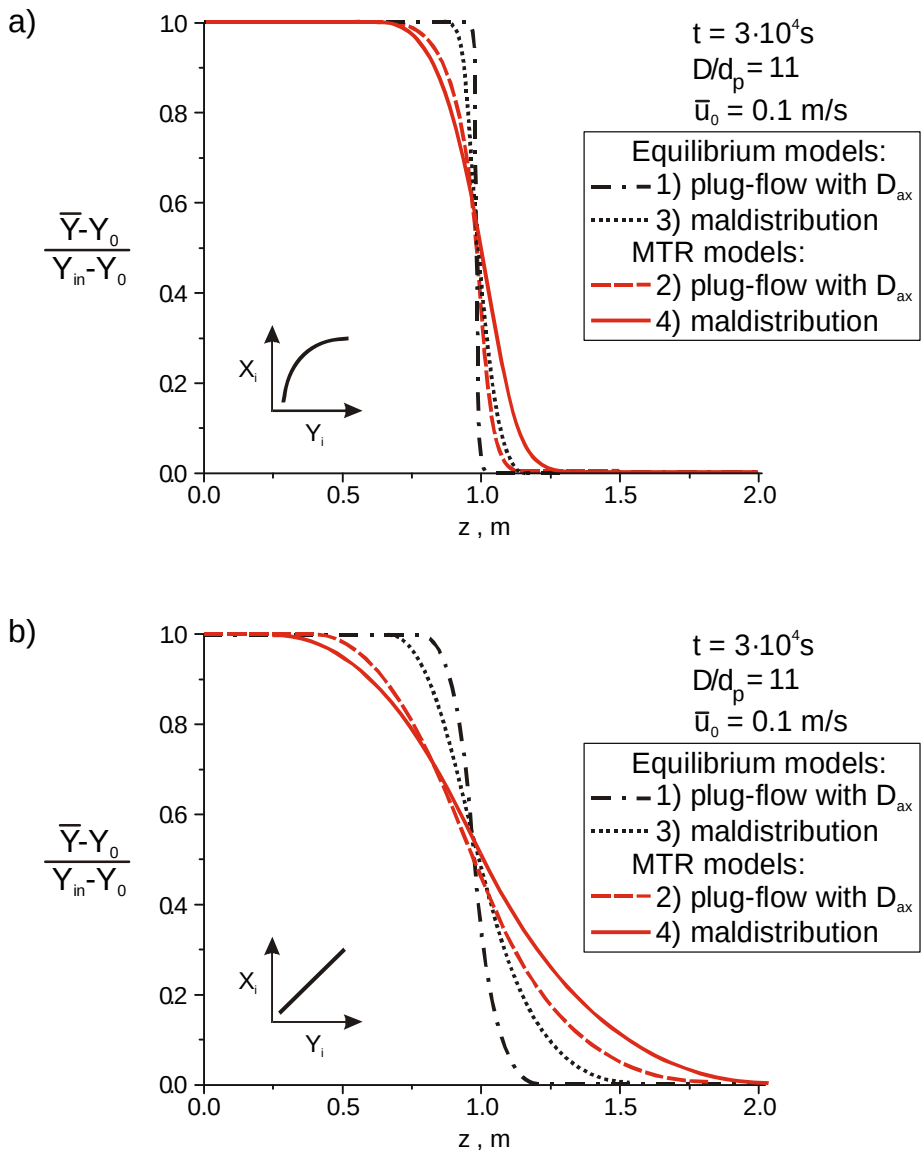

Figure 5. Comparison of axial profiles of average gas moisture content calculated after the various models in case of favorable (a) and throughout linear equilibrium (b); Calculations were made for otherwise the same conditions as in Fig. 3.

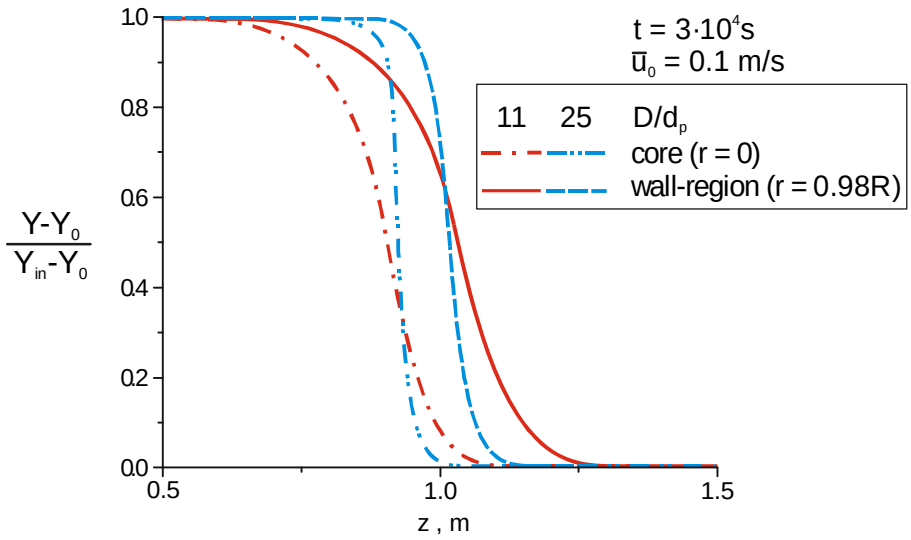

Figure 6. Wall and core profiles of gas moisture content for the isothermal maldistribution model with mass transfer resistance at different tube-to-particle diameter ratios. Calculations were made for the same conditions as in Fig. 3.

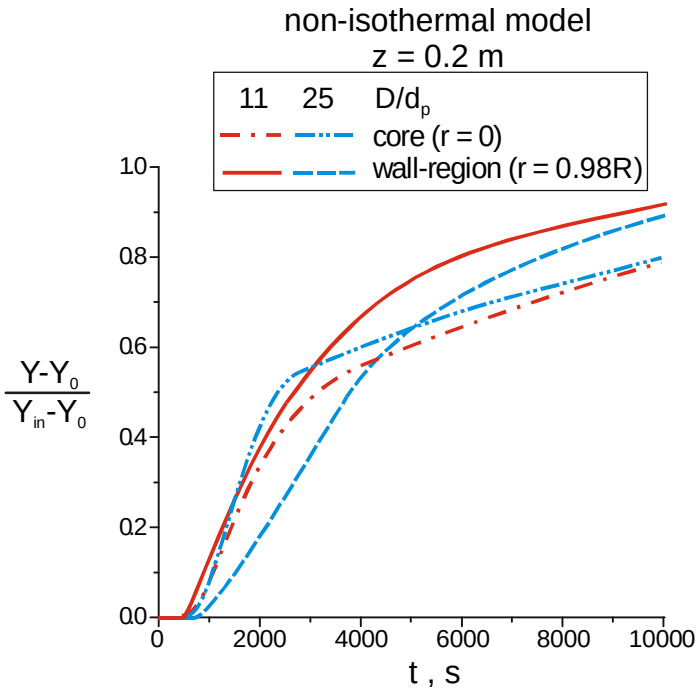

Figure 7. Comparison of wall and core breakthrough curves for different tube-to-particle diameter ratios according to the non-isothermal model.

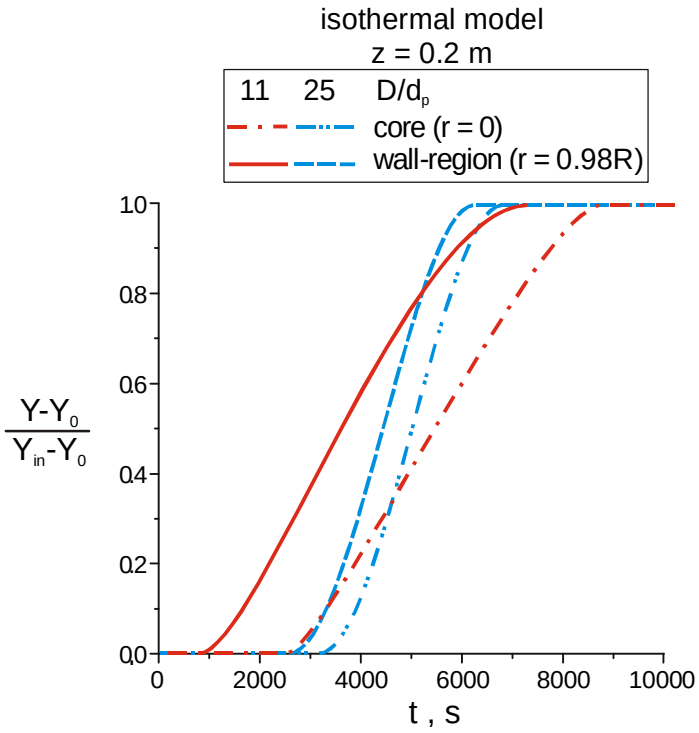

Figure 8. Wall and core breakthrough according to the isothermal version of the maldistribution model.

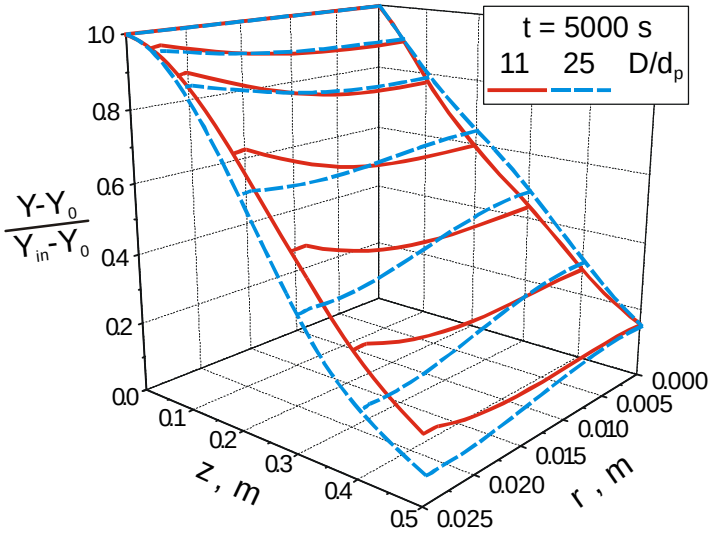

Figure 9. Calculations of gas moisture content field in the adsorber for the non-isothermal maldistribution model with mass transfer resistance, for D/d_p = 11 and D/d_p = 25, at t = 5000 s.

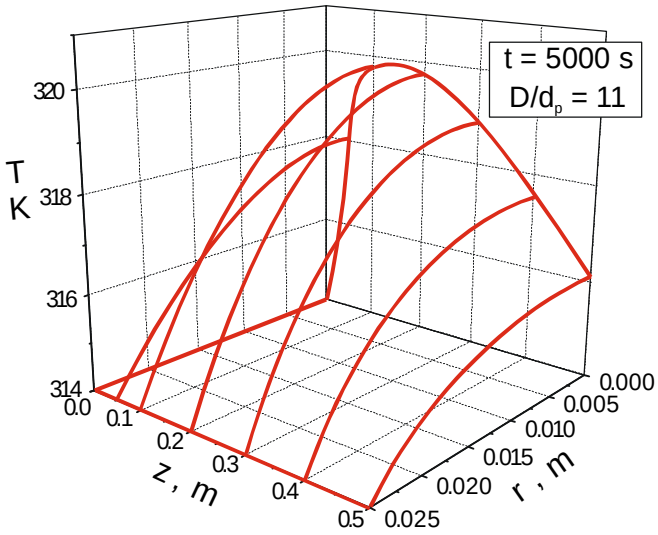

Figure 10. Temperature field in the adsorber according to the non-isothermal maldistribution model with mass transfer resistance for t = 5000 s and $D/d_p = 11$.